Received: 10 March 2021 | Revised: 31 August 2021

DOI: 10.1111/sapm.12465

STUDIES IN APPLIED MATHEMATICS WILEY

ORIGINAL ARTICLE

Traveling waves, blow-up, and extinction in the Fisher–Stefan model

Scott W. McCue | **Maud El-Hachem** | **Matthew J. Simpson**

School of Mathematical Sciences, Queensland University of Technology, Brisbane, Queensland, Australia

Correspondence
Scott W. McCue, School of Mathematical Sciences, Queensland University of Technology, Brisbane QLD 4001, Australia.
Email: scott.mccue@qut.edu.au

Funding information
Australian Research Council, Grant/Award Number: DP200100177

Abstract

While there is a long history of employing moving boundary problems in physics, in particular via Stefan problems for heat conduction accompanied by a change of phase, more recently such approaches have been adapted to study biological invasion. For example, when a logistic growth term is added to the governing partial differential equation in a Stefan problem, one arrives at the *Fisher–Stefan* model, a generalization of the well-known Fisher–KPP model, characterized by a leakage coefficient κ which relates the speed of the moving boundary to the flux of population there. This Fisher–Stefan model overcomes one of the well-known limitations of the Fisher–KPP model, since time-dependent solutions of the Fisher–Stefan model involve a well-defined front which is more natural in terms of mathematical modeling. Almost all of the existing analysis of the standard Fisher–Stefan model involves setting $\kappa > 0$, which can lead to either invading traveling wave solutions or complete extinction of the population. Here, we demonstrate how setting $\kappa < 0$ leads to retreating traveling waves and an interesting transition to finite-time blow-up. For certain initial conditions, population extinction is also observed. Our approach involves studying time-dependent solutions of the governing equations, phase plane, and asymptotic

analysis, leading to new insight into the possibilities of traveling waves, blow-up, and extinction for this moving boundary problem. MATLAB software used to generate the results in this work is available on Github.

KEYWORDS
blow-up, extinction, Fisher–KPP equation, moving boundary problem, retreating fronts, sharp-fronted traveling waves, Stefan problem

1 | INTRODUCTION

Moving boundary problems are frequently used to model phenomena in physics, in particular melting/freezing processes where the moving boundary represents a solid/melt interface[1–3] or interfacial flow problems where the moving boundary is the interface between two fluids.[4] In diffusion-dominated processes, a moving boundary can be driven by swelling of one phase, for example, a polymer or a porous material.[5–7] One key motivation from a physics perspective is to use moving boundary problems to describe pattern formation at the interface, such as that which occurs when a crystal forms from a supercooled melt[8,9] or when viscous fingering develops in a Hele–Shaw cell.[10,11] From a mathematical perspective, there is significant interest in studying various asymptotic or singular solutions to these models and their relevance for the underlying physics.[12]

More recently, researchers have formulated a range of moving boundary problems to model the tissue dynamics and the collective motion of biological cells or bacteria.[13–15] In this study, we concerned with one of the more simple such moving boundary problems, for which the governing partial differential equation is the Fisher–KPP equation.[16] Our focus will be on parameter regimes for which the moving boundary retreats toward the population, instead of invading an empty space. Here, the solutions may evolve to traveling waves, undergo extinction, or blow-up in finite time, the latter of which involves the speed of the moving boundary and the slope of the population density both becoming unbounded at the blow-up time. We establish links with ill-posed models for melting/freezing.

In particular, we will study the following dimensionless moving boundary problem:

$$\frac{\partial u}{\partial t} = \frac{\partial^2 u}{\partial x^2} + u(1-u), \quad 0 < x < s(t), \tag{1}$$

$$\frac{\partial u}{\partial x} = 0 \quad \text{on} \quad x = 0, \tag{2}$$

$$u = 0, \quad \frac{ds}{dt} = -\kappa \frac{\partial u}{\partial x} \quad \text{on} \quad x = s(t), \tag{3}$$

$$u(x,0) = F(x), \quad 0 < x < s(0). \tag{4}$$

Here, $u(x,t)$ represents the density of a certain cell type (such as tumor cells or skin cells), which satisfies the Fisher–KPP equation (1).[17,18] In this simple model, cell motility is described by a constant diffusion coefficient, while cell proliferation is governed by the logistic growth term (here the carrying capacity has been scaled to be $u = 1$).[19,20] Extensive discussion and analysis of how to apply the Fisher–KPP equation to experiments in cell biology are provided in Refs. 21–26, for example. The domain for the Fisher–KPP equation (1) is bounded to the right by a moving boundary $x = s(t)$, at which the cell density vanishes. The second condition in (3) is a Stefan-like boundary condition[2] and for this reason we refer to (1)–(4) as the *Fisher–Stefan* model. The parameter κ in (3) is a leakage coefficient that drives the speed of the interface in the same way that a Stefan number does in the analogous Stefan problem. The loss of mass at the moving boundary could be driven by invasion into ($\kappa > 0$) or recession from ($\kappa < 0$) a harsh environment. Alternatively, for $\kappa < 0$, the cell loss could be associated with a conversion of the main cell population into another cell type that is left behind as the front recedes. An argument for how κ could be determined given experimental data is provided in Ref. 27.

The one-phase model (1)–(4) with a single moving boundary sits within a class of Stefan-type moving boundary problems for reaction diffusion models with a linear diffusion term. Much of this work began with Du and Lin,[16] who studied advancing fronts that either go to extinction or evolve to traveling waves. They refer to these two options as leading to a "spreading-vanishing dichotomy." Rigorous results for this one-phase problem were subsequently established for the long-time asymptotics, more general source terms, and the radially symmetric version in higher dimensions by Du and coworkers.[28–30] Since that time, much attention has been devoted to various generalizations, many of which are reviewed by Du.[31] In very recent times, a variety of extensions have been documented, including a rigorous results for different boundary conditions, nonlinear or nonlocal diffusion, generalized reaction terms, with one or two phases, as well as motivation in terms of applications in ecology.[32–45] Formal results and numerical simulations have been described by us[27,46–49] and others.[50]

Most of the key results for the core Fisher–Stefan model (1)–(4) hold for $\kappa > 0$, for which the moving boundary $x = s(t)$ moves in the positive x-direction. For example, with $\kappa > 0$ and provided $s(0) > \pi/2$, the time-dependent solution of (1)–(4) will evolve toward a traveling wave profile with a speed $0 < c < 2$ that depends on κ, with $c \to 0^+$ as $\kappa \to 0^+$ and $c \to 2^-$ as $\kappa \to \infty$.[16,31,46] This interval of c values for the Fisher–Stefan model is surprising because solutions of the traditional Fisher–KPP equation on $0 < x < \infty$ evolve to traveling wave profiles with speeds $c > 2$ and the traveling wave profiles for $0 < c < 2$ (whose trajectories in the phase plane have spiral at the origin) are normally discarded as being unphysical, since they involve negative population densities for sufficiently large values of the independent variable $z = x - ct$. A stronger result for (1)–(4) is that if $s(t)$ ever becomes greater than $\pi/2 - \kappa \int_0^{s(t)} u(x,t)\,dx$ then the traveling wave is guaranteed.[46] Alternatively, for $s(0) < \pi/2$ and $u(x,0) = F(x)$ sufficiently small, the solution goes extinct with $u(x,t) \to 0$, $s(t) \to s_e$ as $t \to \infty$, where $s(0) < s_e < \pi/2$ is a constant.[16,31,46] This behavior is interesting because solutions of the Fisher–KPP equation on $0 < x < \infty$ with a no-flux condition at $x = 0$ do not ever go extinct. Together the above results are referred to by Du and coworkers as the spreading-vanishing dichotomy.[16,31]

Much less attention has been devoted to (1)–(4) for $\kappa < 0$.[27,48] Here, the moving boundary $x = s(t)$ propagates in the negative x-direction. For $-1 < \kappa < 0$, we have previously shown that, for sufficiently large $s(0)$, solutions to (1)–(4) very quickly evolve toward receding traveling wave profiles that persist as long as $s(t) \gg 1$ (ultimately the no-flux condition at $x = 0$ will disturb this trend).[27] These traveling wave solutions move with speed $c \sim \kappa/\sqrt{3}$ as $\kappa \to 0$ and $c \sim -2^{-1}(1+\kappa)^{-1/2}$ as

$\kappa \to -1^+$; their profiles correspond to portions of trajectories in the phase plane that emerge from a saddle point (but are not heteroclinic orbits). An exact solution for $c = -5/\sqrt{6}$ can be written down in terms of the equianharmonic case of the Weierstrass p-function.[48,51] There is a stationary wave solution for $\kappa = 0$, which corresponds to a homoclinic orbit in the phase plane.[27] Again, all of these traveling wave trajectories for $c \leq 0$ are normally discarded as being unphysical, as their full trajectories in the phase plane involve negative population densities. Note the shape of the traveling wave profiles for $-1 < \kappa < 0$ are qualitatively similar to those for $\kappa > 0$, except that they become steeper as κ decreases.

In Section 2 of the paper, we are mostly concerned with presenting new results for the parameter regime $\kappa < -1$, $s(0) \gg 1$, for which a phase-plane analysis shows there are no traveling wave solutions. We demonstrate that time-dependent solutions to (1)–(4) can blow up in finite time for $\kappa < -1$, with $ds/dt \to -\infty$ as $t \to t_c$, and conjecture that for the borderline case $\kappa = -1$ the blow up is at infinite time. These results are interesting because this type of blow up has not ever been observed before for models with the Fisher–KPP equation. For $s(0) = \mathcal{O}(1)$, in Section 3 we rescale the problem to compare with a well-studied ill-posed Stefan problem for melting a superheated solid (or freezing a supercooled liquid). In this case, as well as the option of blow-up in finite time, solutions may go to extinction, whereby the population approaches zero in a nonzero domain in the long time limit. We argue that for $s(0) = \mathcal{O}(1)$, the critical value of κ that separates blow-up from extinction depends on the initial population and a parameter that measures cell proliferation (this parameter is equal to $s(0)^2$ in the version of the problem (1)–(4)). Furthermore, we provide estimates for the distance the moving boundary travels before the solution goes to extinction. As such, we provide new links between the Fisher–Stefan moving boundary model with ill-posed Stefan problems. Finally, we provide concluding remarks in Section 4. Full details of our numerical scheme are provided in Appendix A, while MATLAB software to solve the time-dependent PDE models in this work is available on Github.

2 | TRAVELLING WAVES AND BLOW-UP FOR $s(0) \gg 1$

2.1 | Time-dependent solutions

In this section, we explore the time-dependent behavior of solutions to (1)–(4) for cases in which $s(0) \gg 1$. The motivation here is to observe the solution evolving to a traveling wave profile ($-1 < \kappa < 0$) or blowing up in finite time ($\kappa < -1$). Provided that $s(t) \gg 1$, the consequences of imposing the no-flux condition (2) are negligible (thus, in effect, we are treating (1)–(4) on $-\infty < x \leq s(t)$).

For that purpose, we use the initial condition

$$F(x) = \alpha(1 - \mathrm{H}(s(0))), \tag{5}$$

which is simply a step function, where $\mathrm{H}(x)$ is the Heaviside function and $\alpha > 0$ is a parameter that stipulates the initial density. A crucial step for our numerical scheme is to map $0 < x < s(t)$ to a fixed domain $0 < y < 1$ via $y = x/s(t)$. The solutions we are interested in turn out to be very steep near $x = s(t)$ ($y = 1$) and very flat near $x = 0$ ($y = 0$), and so it proves useful to discretize the unit interval in y with an uneven mesh such that the grid points are increasing close together as y increases. For most of the simulations in this paper we use $N = 1001$ grid points so that the

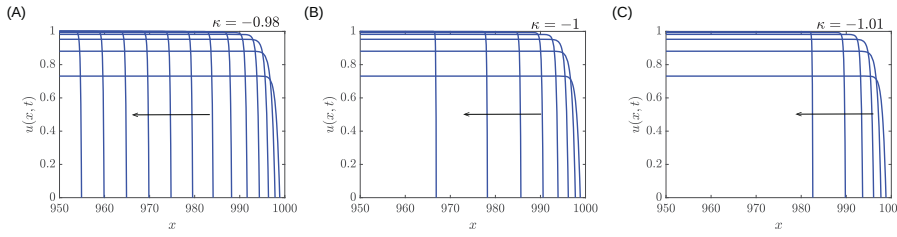

FIGURE 1 Time-dependent solutions of (1)–(4) for three different values of κ: (A) $\kappa = -0.98$; (B) $\kappa = -1$; and (C) $\kappa = -1.01$. In each case, we have use the initial condition (5) with $\alpha = 0.5$ and $s(0) = 1000$. The solutions are drawn at unit time intervals up to (A) $t = 13$, (B) $t = 8$, and (C) $t = 6$. These three examples are representative of solutions that appear to (A) evolve to a traveling wave, (B) blow up in infinite time, and (C) undergo finite-time blow-up

smallest grid spacing near $y = 1$ is 1×10^{-6}. The details of the numerical scheme are recorded in Appendix A.

In Figure 1, we show numerical solutions for three different values of leakage coefficient κ, all computed with the initial condition (5) with $\alpha = 0.5$ and $s(0) = 1000$. In panel A, the solution for $\kappa = -0.98$ is representative of solutions for $-1 < \kappa < 0$. Here, as the interface $x = s(t)$ begins to propagate in the negative x-direction, the maximum value of u begins to rise from $u = 0.5$ at $t = 0$ toward $u = 1$, and the solution appears to evolve to a constant shape moving from right to left with constant speed (the solutions are drawn at equally spaced times $t = 0, 1, 2, ...$). Indeed, as demonstrated in El-Hachem et al,[27] this solution is evolving toward a traveling wave profile that we explore further in Subsection 2.2. Of course, this convergence to a traveling wave cannot continue indefinitely, as we have imposed a no-flux condition at $x = 0$ in our numerical scheme; however, these almost-traveling-wave profiles persist until $s(t) = \mathcal{O}(1)$. We defer a discussion about the effects of (2) until Section 3. Note that this qualitative behavior we see in Figure 1 for the initial condition with $\alpha = 0.5$ is observed for all $0 < \alpha < 1$.

Figure 1B–C contains two more numerical solutions, one for $\kappa = -1$ and the other for $\kappa = -1.01$. These solutions are for parameter values not considered previously in the literature. In both cases, the solution does not appear to evolve to a traveling wave. In panel B, with $\kappa = -1$, it is clear the speed of the interface continues to increase as time progresses (again, the solutions are drawn at equally spaced times), while in panel C, with $\kappa = -1.01$, this trend is also apparent, although this figure does not show what happens for latter times. We defer further discussion on these solutions for $\kappa \leq -1$ until Subsection 2.3.

2.2 | Traveling wave solutions, $-1 < \kappa < 0$

In this subsection, we briefly review the key results for the existence of traveling wave solutions for the parameter range $-1 < \kappa < 0$.[27] With this in mind, we write $u = U(z)$, where z is the traveling wave coordinate $z = x - ct$, so that U satisfies

$$\frac{d^2U}{dz^2} + c\frac{dU}{dz} + U(1 - U) = 0. \tag{6}$$

Here, c is the speed of the traveling wave solution.

For the physically relevant boundary conditions we have in mind here, namely,

$$U \to 1^-, \quad \frac{dU}{dz} \to 0^-, \quad \text{as} \quad z \to -\infty, \tag{7}$$

most studies of (6) are for $c > 0$. In that case, traditional traveling wave solutions to the Fisher–KPP equation, for $c \geq 2$, correspond to heteroclinic orbits that join the saddle point representing (7) with the origin $U = 0$, $dU/dz = 0$. As mentioned in Section 1, for the Fisher–Stefan problem (1)–(4) with $\kappa > 0$ and sufficiently large initial values of $s(0)$, solutions evolve to traveling wave solutions for $0 < c < 2$; these correspond to the portion of the heteroclinic orbit joining the saddle and the origin that has $U \geq 0$, $dU/dz \geq 0$.

Turning now to the regime we are interested in here, namely, $c < 0$. In this case, we let $V = -dU/dz$, so that (6) is rewritten as the coupled system of first-order equations

$$\frac{dU}{dz} = -V, \tag{8}$$

$$\frac{dV}{dz} = -cV + U(1 - U). \tag{9}$$

The phase plane (U, V) is simply a reflection of the traditional representation about the U-axis. As such, the qualitative behavior of trajectories carries over from before. That is, for $-2 < c < 0$ the equilibrium point at the origin is a spiral, just like that for $0 < c < 2$ except for the reflection, while the origin for $c \leq -2$ is a node as with $c \geq 2$, again with reflection.

We demonstrate these ideas with four examples in Figure 2, drawn for the different values of $c = -0.1$, -1, -2, and -5. These results are found by solving (8)–(9) numerically using Heun's method with a constant step size dz. In each case shown in this figure, we have drawn (thick, red) the portions of the phase plane that correspond to the traveling wave solutions we are concerned with. These all begin at $(U, V) = (0, 0)$ and traverse the fourth quadrant until they intersect the V-axis at some special value, $V = V^*$ say. For the four examples presented in Figure 2, the numerical estimates of V^* are (A) $c = -0.1$, $V^* = -0.643$, (B) $c = -1$, $V^* = -1.32$, (C) $c = -2$, $V^* = -2.21$, and (D) $c = -5$, $V^* = -5.10$. Given the Stefan condition (3), we know that $c = -\kappa V^*$, so these numerical estimates in the phase plane correspond to panels (A) $\kappa = -0.156$, (B), $\kappa = -0.753$, (C) $\kappa = -0.904$, and (D) $\kappa = -0.981$. For each of these κ values, our numerical simulations show that time-dependent solutions of the full Fisher–Stefan model (1)–(4) with $s(0) \gg 1$ evolve toward the traveling wave profiles with the predicted values of c.

For completeness, we also show in Figure 2a number of trajectories (thin, purple) that do not begin at the saddle point at $(U, V) = (1, 0)$ and so do not satisfy (7). None of these are physically-relevant traveling wave solutions. We have also shown the trajectories that represent either invading traveling wave solutions (thick, green). For panels A–B, for which the values of c lie in the interval $-2 < c < 0$, these trajectories are normally discarded since the spirals involve negative portions of the population; however, for the Fisher–Stefan model (1)–(4) with $\kappa > 0$, these are truncated at when they first meet the V-axis. For panels C–D, for which $c \leq -2$, the invading traveling wave trajectories (thick, green) represent traditional traveling wave solutions to the Fisher–KPP equation.

It is easy to see that the solutions of (6) for $c < 0$ that satisfy (7) (corresponding to the thick red curves in Figure 2) exist for $-\infty < c < 0$. In the limit $c \to -\infty$, we see from (8)–(9) that $dV/dU = -c + U(1 - U)/V \sim -c$ which suggests the relevant trajectories in the phase-plane

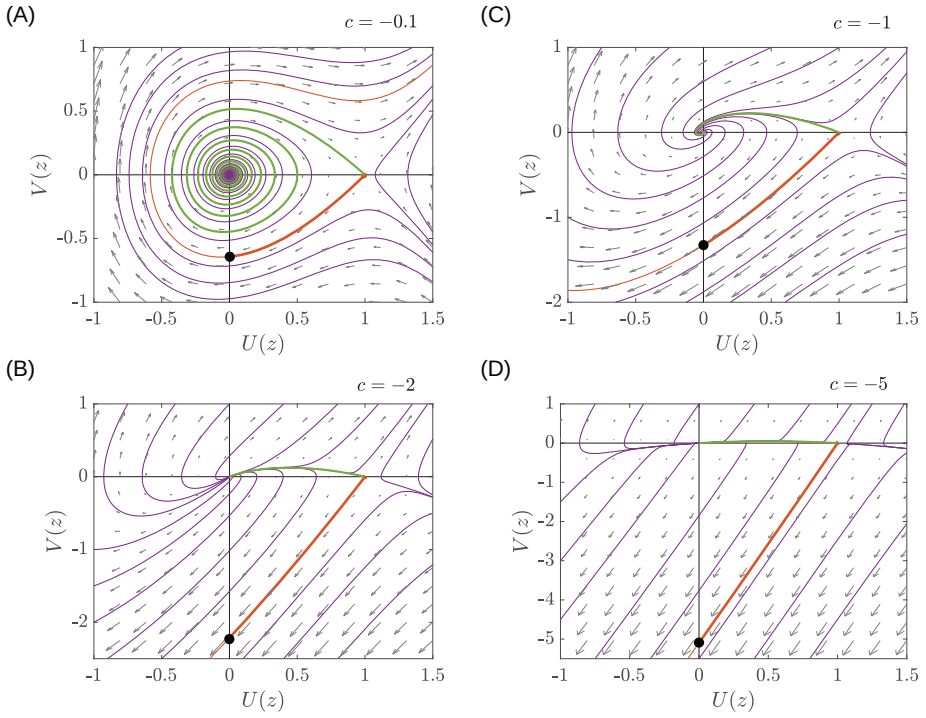

FIGURE 2 Representative phase planes for (A) $c = -0.1$, (B) -1, (C) -2, and (D) -5, drawn by numerically integrating (8)–(9). In each case, the thick trajectory in red represents the solution to (6) that satisfies the far-field condition (7). These trajectories are truncated at the V-axis at some value $V = V^*$ (indicated by the solid black disc) which allows for the numerical prediction of κ via $c = -\kappa V^*$, thereby linking these traveling wave profiles with the intermediate-time solutions to the moving boundary problem (1)–(4). Note the green thick trajectories are the heteroclinic orbits that connect the saddle point $(U, V) = (1, 0)$ with the fixed point at the origin

approach the straight lines $V = c(U - 1)$. Given $V^* = V|_{U=0}$, we have $\kappa \to -1^+$ as $c \to -\infty$. In El-Hachem et al, [27] we derive the approximation

$$U \sim 1 - \mathrm{e}^{-cz} + \frac{\mathrm{e}^{-cz}(2cz - 1 + \mathrm{e}^{-cz})}{2c^2} \quad \text{as} \quad c \to -\infty, \tag{10}$$

which leads to the limiting behavior $\kappa \sim -1 + (2c^2)^{-1}$ as $c \to -\infty$ or, in other words, $c \sim -2^{-1}(1 + \kappa)^{-1/2}$ as $\kappa \to -1^+$.

2.3 | Finite-time blow up, $\kappa < -1$

The previous subsection summarizes recently recorded results for values of the leakage coefficient in the interval $-1 < \kappa < 0$, for which time-dependent solutions of (1)–(4) evolve to traveling waves. Since the phase-plane analysis in that subsection does not apply for $\kappa \leq -1$, we are now motivated to explore the time-dependent behavior of solutions in this parameter regime.

Returning to Figure 1, the solutions in panels B and C do not appear to approach a traveling wave like the solution in panel A. For example, the moving boundary in panel B ($\kappa = -1$) appears

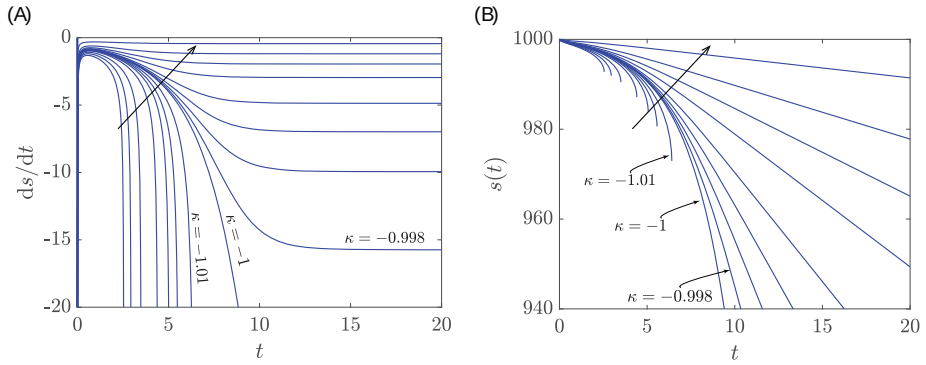

FIGURE 3 Numerical results for (1)–(4) showing the dependence of (A) the speed of the moving boundary ds/dt and (B) location of the moving boundary $s(t)$ versus t. The arrows indicate increasing values of κ. From bottom left to top right, the solutions are drawn for $\kappa = -1.2, -1.15, -1.1, -1.05, -1.03, -1.02, -1.01, -1, -0.998, -0.995, -0.99, -0.98, -0.95, -0.9, -0.8$, and -0.5

to move a longer distance at each time-interval, remembering that each solution is drawn at unit intervals $t = 0, 1, 2, \ldots$. The largest time shown in Figure 1B is $t = 7$ and indeed the location of the moving boundary for $t = 8$ is too far to the left to fit on the figure. Similarly, for the solution in panel C ($\kappa = -1.01$), the largest time shown is $t = 5$ since the solution for $t = 6$ does not fit on this scale.

To further explore the ultimate behavior of these solutions, we present in Figure 3A plots of the speed of the moving boundary $x = s(t)$ versus time for various values of κ. For the eight examples with $-1 < \kappa < 0$, we clearly see the speed leveling off to a constant value as time increases, supporting our observations that solutions in this parameter regime evolve to traveling waves. On the other hand, for the six examples with $\kappa < -1$, the speed appears to approach a vertical asymptote, suggesting there is a form of finite-time blow-up with $ds/dt \to -\infty$ as $t \to t_c^-$. For instance, for $\kappa = -1.01$, corresponding to the solution in Figure 1C, the blow-up time appears to be roughly $t_c \approx 6.4$.

A slightly different perspective is provided by plotting the moving boundary location $s(t)$ versus time t, as in Figure 3B. Here, we see solutions for $-1 < \kappa < 0$ evolve to straight lines with nonzero slopes that correspond to the traveling wave speeds, while solutions for $\kappa < -1$ appear to truncate at finite values of s at the finite blow-up time, which suggests that $s \to s_c^+$ as $t \to t_c^-$. For the particular example $\kappa = -1.01$, the numerical estimate for the end point is $s_c \approx 975$.

It is useful to explore the scalings in the blow-up limit $t \to t_c^-$. We plot in Figure 4 the dependence of $\ln(-ds/dt)$ and $\ln(s(t) - s_c)$ versus $\ln(t_c - t)$. On this scale, it appears that in both panels A and B the curves are roughly linear with slope $-1/2$, suggesting a power-law relationship in the limit. We return to this issue in Section 3.

The shape of the solution at blow-up appears to be qualitatively similar to that for times leading up to blow-up. For example, for the simulation shown in Figure 1C, where we have $\kappa = -1.01$, the numerical estimate of the blow-up profile is included in Figure 5 as a solid blue curve. This numerical solution is computed very slightly before the estimated blow-up time, which is $t_c \approx 6.4$. While it is difficult to appreciate the difference between this solution and those for previous times, the key point is that this form of blow-up is characterized by the slope of the solution becoming infinite at $x = s(t)$ where $u(s(t), t) = 0$. A simple estimate of the solution near blow-up for $\kappa \sim -1^-$ can be written down by looking for a solution $u \sim w(\zeta)$, where $\zeta = \dot{s}(x - s(t))$, assuming

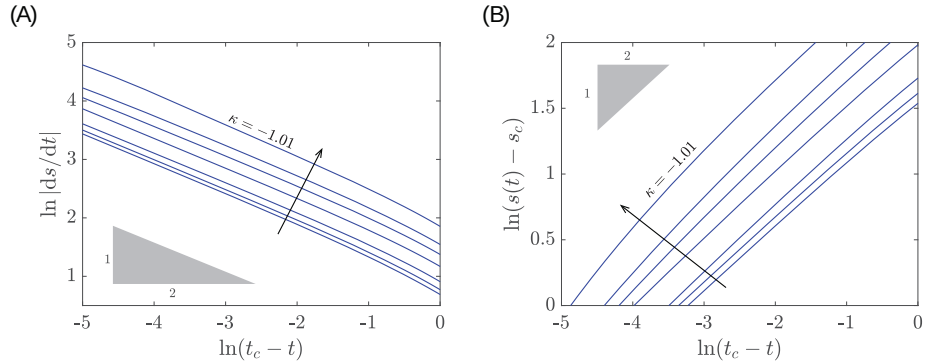

FIGURE 4 Log–log plots for (A) ds/dt versus $t_c - t$ and (B) $s(t) - s_c$ versus $t_c - t$, drawn for $\kappa = -1.2$, -1.15, -1.1, -1.05, -1.02, and -1.01. Also included is a line segment with slope $-1/2$

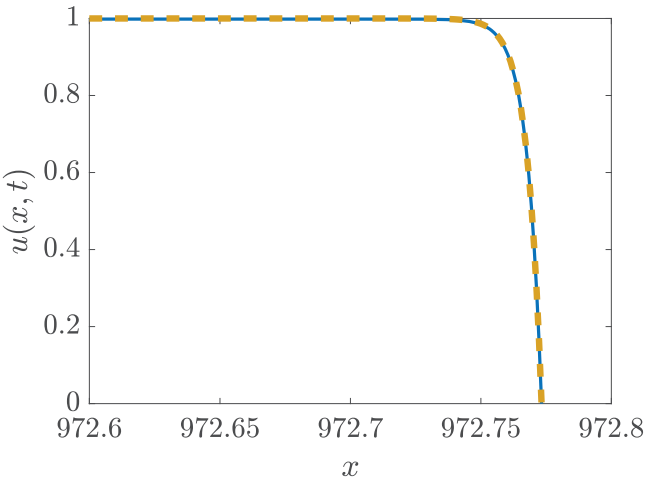

FIGURE 5 Numerical solution very close to blow-up. The solid blue curve is the numerical solution of (1)–(4) for $\kappa = -1.01$, $t = 6.41$, for which $s \approx 972.78$ and $\dot{s} \approx -183.78$. The dashed orange curve is the estimate (11) computed using these values

$|\dot{s}^2| \gg |\ddot{s}| \gg 1$ (which is true if $s(t) - s_c \sim (t_c - t)^{1/2}$ or similar, for example). Then, to leading order, (1) gives $-w' \sim w''$, whose solution is $w = A + B\,e^{-\zeta}$, where A and B are constants. By fixing $w = 0$ at $\zeta = 0$ and matching back to $w = 1$ as $\zeta \to -\infty$, we find

$$u \sim 1 - e^{-\dot{s}(x - s(t))} \quad \text{as} \quad t \to t_c^-, \quad \kappa \sim -1^-. \tag{11}$$

We plot this simple profile in Figure 5 using the numerical values of $\dot{s}$ and s for this particular value of t. The agreement is quite good.

Having established strong numerical evidence for traveling wave outcomes for $-1 < \kappa < 0$ and finite-time blow-up for $\kappa < -1$, it remains to consider the borderline case $\kappa = -1$. In this instance, we conjecture that the solution undergoes infinite-time blow-up. As mentioned above, in Figure 1B we see the solution front appearing to increase its speed with time, and that observation is confirmed in Figure 3, where both $|ds/dt|$ and $|s(t)|$ appear to continue to increase with time. These numerical results support infinite-time blow-up. Furthermore, from our phase-plane analysis of traveling wave solutions in Subsection 2.2 and El-Hachem et al,[27] we find the traveling

wave speeds has the limiting behavior $c \sim -2^{-1}(1+\kappa)^{-1/2}$ as $\kappa \to -1^+$, which provides further analytical evidence for our conjecture.

3 | BLOW-UP VERSUS EXTINCTION FOR $s(0) = \mathcal{O}(1)$

3.1 | Preamble

We turn now to studying (1)–(4) for cases in which $s(0) = \mathcal{O}(1)$. Here, the no-flux condition (2) is important and cannot be ignored.

It proves convenient to rescale our problem by introducing the new variables $\tilde{x} = x/s(0)$, $\tilde{t} = t/s(0)^2$, and $\tilde{s}(\tilde{t}) = s(t)/s(0)$, so that (1)–(4) becomes

$$\frac{\partial \tilde{u}}{\partial \tilde{t}} = \frac{\partial^2 \tilde{u}}{\partial \tilde{x}^2} + \lambda \tilde{u}(1-\tilde{u}), \quad 0 < \tilde{x} < \tilde{s}(\tilde{t}), \tag{12}$$

$$\frac{\partial \tilde{u}}{\partial \tilde{x}} = 0 \quad \text{on} \quad \tilde{x} = 0, \tag{13}$$

$$\tilde{u} = 0, \quad \frac{d\tilde{s}}{d\tilde{t}} = -\kappa \frac{\partial \tilde{u}}{\partial \tilde{x}} \quad \text{on} \quad \tilde{x} = \tilde{s}(\tilde{t}), \tag{14}$$

$$\tilde{u}(\tilde{x}, 0) = \tilde{F}(\tilde{x}), \quad 0 < \tilde{x} < 1, \tag{15}$$

where the two parameters in the problem are now κ (as before) and

$$\lambda = s(0)^2. \tag{16}$$

Note that the spatial domain is now a subset of [0,1] so that for $\lambda = \mathcal{O}(1)$ the no-flux condition (13) plays an important role. In particular, in this parameter regime, solutions do not evolve to traveling waves, but instead appear to either undergo finite-time blow-up or go to extinction, as we demonstrate.

3.2 | Model for melting a superheated solid

The reformulation in Subsection 3.1 has the advantage of setting up a direct analogy with a well-studied problem for melting a superheated solid (or freezing a supercooled liquid), as we now summarize. Consider (12)–(15) with $\lambda = 0$. In this case, the moving boundary problem has the following interpretation.[12,52–58] First, $\tilde{u}(\tilde{x}, \tilde{t})$ is the (dimensionless) temperature of a superheated solid on the domain $0 < \tilde{x} < \tilde{s}(\tilde{t})$, where the melting temperature is scaled to be $\tilde{u} = 0$. Here, $\tilde{x} = \tilde{s}(\tilde{t})$ is the interface between the solid phase $0 < \tilde{x} < \tilde{s}(\tilde{t})$ and the liquid phase $\tilde{x} > \tilde{s}(\tilde{t})$, the latter being assumed to remain at the melting temperature for all time. The first condition in (14) enforces continuity of temperature across the domains, while the second is a Stefan condition that balances heat conducting in to the interface with energy required to melt the solid. Remembering that $\kappa < 0$, this balance is characterized by the Stefan number $\beta = -1/\kappa$, which is a ratio of the

latent heat per unit mass at the equilibrium temperature with a product of the specific heat of the solid and a representative temperature scale.

The one-phase Stefan problem (12)–(15) with $\lambda = 0$ is nonclassical because the initial temperature $\tilde{F}(\tilde{x})$ is positive, which means the solid is superheated. Here, the solid-melt interface $\tilde{x} = \tilde{s}(\tilde{t})$ is driven to move in the negative $\tilde{x}$-direction as the solid melts. Such a scenario is particularly unstable and so this simplified model, which is ill-posed, is highly idealized. In the classical case, for which the initial temperature is negative, the interface would move in the positive $\tilde{x}$-direction. Note that by replacing $\tilde{u}$ with $-\tilde{u}$, the model (12)–(15) with $\lambda = 0$ is for freezing a supercooled liquid, such as that which occurs with diffusion-limited dendritic solidification. Therefore, the behavior of the interface $\tilde{x} = \tilde{s}(\tilde{t})$ that we describe for the superheated solid also applies for the equivalent problem for a supercooled liquid.

It is known that there are three qualitatively different outcomes for (12)–(15) with $\lambda = 0$.[12,52–54,57,58] The first is incomplete melting of the solid, whereby the solution exists for all time with $\tilde{s} \to \tilde{s}_{\rm e}^{+}$ and $\tilde{u}(\tilde{x}, \tilde{t}) \to 0^{+}$ as $\tilde{t} \to \infty$. The second is complete melting of the solid, where $\tilde{s}(\tilde{t}_{\rm e}) = 0$ for a finite time $\tilde{t}_{\rm e}$. Finally, the third possible outcome is a finite-time blow-up of the type we have studied in Subsection 2.3, whereby the solution exists up to some time $\tilde{t}_{\rm c}$, with $\tilde{s} \to \tilde{s}_{\rm c}^{+}$ and $d\tilde{s}/d\tilde{t} \to -\infty$ as $\tilde{t} \to \tilde{t}_{\rm c}^{-}$. To help classify possible solutions, the superheating parameter

$$Q = \int_0^1 \tilde{F}(\tilde{x})\, d\tilde{x} + \kappa^{-1} \tag{17}$$

is useful. Here, Q is the sum of the amount of heat that is required to be removed from the solid to reduce the temperature from $\tilde{u} = \tilde{F}(\tilde{x})$ to $\tilde{u} = 0$ and the latent heat which must be absorbed at the interface to melt the solid (remembering that no heat can enter the system from the left-hand boundary $\tilde{x} = 0$). A simple result is that the third qualitative outcome (finite-time blow-up) will always occur if $Q > 0$, as the initial heat energy in the solid is greater than what is required to melt it, leaving a surplus of energy which cannot conduct away or leave the system. Another is if $\tilde{F}(\tilde{x})$ is smooth and monotonic with $\tilde{F}(1) = 0$, then $Q < 0$ leads to the first qualitative outcome, as there is not enough heat initially in the solid to convert to the latent heat required to melt the entire solid, while $Q = 0$ is the borderline case in which there is precisely the right amount of initial heat to melt the entire solid and the region melts completely in finite time.

To explore these results further, we integrate (12) with $\lambda = 0$ and combine with (13)–(15) to give

$$\tilde{s}(\tilde{t}) = -\kappa(M(\tilde{t}) - Q), \tag{18}$$

where $M(\tilde{t})$ is the amount of heat in the solid at a given time,

$$M(\tilde{t}) = \int_0^{\tilde{s}(\tilde{t})} \tilde{u}(\tilde{x}, \tilde{t})\, d\tilde{x}.$$

Then, for $Q < 0$ with incomplete melting, whereby $\tilde{s} \to \tilde{s}_{\rm e}^{+}$ and $\tilde{u}(\tilde{x}, \tilde{t}) \to 0^{+}$ as $\tilde{t} \to \infty$, we can predict that $\tilde{s}_{\rm e} = \kappa Q$ or, alternatively[12,52–58]

$$\tilde{s}_{\rm e} = 1 + \kappa M(0), \quad \text{for } Q < 0 \quad \text{(incomplete melting)} \tag{19}$$

We demonstrate this behavior in Figure 6 where we show time-dependent solutions of (12)–(15) with $\lambda = 0$ for an initial condition $\tilde{u}(\tilde{x}, 0) = M(0)$, $0 \le \tilde{x} \le 1$. In Figure 6A, we have set $M(0) = 1$

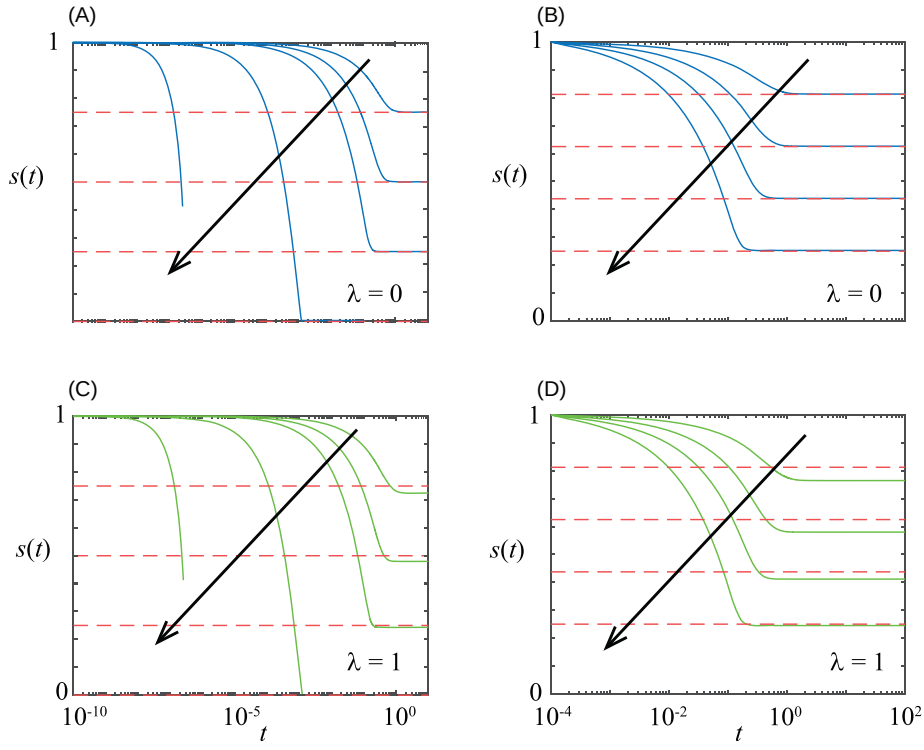

FIGURE 6 Numerical solutions of (12)–(15) presented in terms of $\tilde{s}(\tilde{t})$ with for $\tilde{s}(0) = 1$. (A) $M(0) = 1$ with $\kappa = -0.25$ ($Q = -3$), -0.5 ($Q = -1$), -0.75 ($Q = -0.333$), -1 ($Q = 0$), and -1.25 ($Q = 0.2$), with the arrow showing the direction of decreasing κ. (B) $\kappa = -0.75$ with $M(0) = 1$ ($Q = -0.333$), 0.75 ($Q = -0.583$), 0.5 ($Q = -0.833$), and 0.25 ($Q = -1.083$), with the arrow showing the direction of increasing $M(0)$. Results in panels C–D are the same as in panels A–B, respectively, except that $\lambda = 1$. In each subfigure, we show a red dashed line indicating $\tilde{s}_e = \kappa Q$, which is the predicted final position of the moving boundary when $\lambda = 0$ (except for the cases $M(0) = 1$, $\kappa = -1.25$, for which the prediction $\tilde{s}_e < 0$)

and used the leakage coefficient values $\kappa = -0.25, -0.5, -0.75, -1$, and -1.25. Here, the predicted final positions of the moving boundary are $\tilde{s}_e = 0.75$, 0.5, 0.25, 0, and -0.25, respectively. For the first four of these cases, the numerical simulations agree well with the analytical prediction. For the last case, $\kappa = -1.25$, the prediction $\tilde{s}_e = -0.25$ is unphysical; however, here $Q > 0$ and so instead the solution undergoes finite-time blow-up, as described above. Similarly, in Figure 6B, we show results for $\kappa = -0.75$ with $M(0) = 1$, 0.75, 0.5, and 0.25. In this case, the predicted values of $\tilde{s}_e$ are 0.25, 0.4375, 0.625, and 0.8125, respectively. Again, the numerical simulations agree well with the analytical results.

3.3 | Time-dependent results for $\lambda > 0$

The case in which $\lambda > 0$ is fundamentally different because the logistic growth term in (12) acts to increase the total population, making the full problem (12)–(15) with $\lambda > 0$ more complicated than that with $\lambda = 0$, especially in terms of analytical predictions. Results in Figure 6C–D are presented in the same format as those in Figure 6A–B except that we set $\lambda = 1$. Here, we see

that the formula for $\tilde{s}(\tilde{t})$ given by (18) (which is for $\lambda = 0$) underestimates the distance interface moves. This observation agrees with our intuition that the source term in (12) increases the total population, so the front moves further toward the origin before extinction.

As a first step toward understanding the extinction behavior with $\lambda > 0$ we approximate (12)–(15) by neglecting the quadratic term, so that we are working with an analog of Skellam's equation.[59] In this case, assuming that the population goes to extinction (that is, $\tilde{s} \to \tilde{s}_e^+$ and $\tilde{u}(\tilde{x}, \tilde{t}) \to 0^+$ as $\tilde{t} \to \infty$), then we obtain

$$\tilde{s}_e = \kappa\left(Q + \lambda \int_0^\infty M(t)\, dt\right) \quad \text{for extinction.} \tag{20}$$

Since the integral is positive and $\kappa < 0$, this expression confirms that $\tilde{s}_e$ decreases with λ, consistent with our numerical explorations in Figure 6, where we compared results for $\lambda = 0$ with those for $\lambda = 1$. Interestingly, for the case $M(0) = 1$, $\kappa = -1$ in Figure 6A ($\lambda = 0$), we have the exact prediction $\tilde{s}_e = 0$, while for $M(0) = 1$, $\kappa = -1$ in Figure 6C ($\lambda = 1$), our approximate result (20) has $\tilde{s}_e < 0$, which is unphysical and implies the solution blows up in finite time. This result demonstrates how increasing λ results in a transition from extinction to blow-up.

3.4 | Blow-up revisited

As discussed above, for the Stefan problem (12)–(15) with $\lambda = 0$, the exact result (19) holds provided $Q < 0$ and the solutions goes to extinction ($\tilde{u} \to 0$ as $\tilde{t} \to \infty$ for all $0 < \tilde{x} < \tilde{s}_e$). Similarly, the borderline case occurs when $Q = 0$ and $\tilde{s}_e = 0$. On the other hand, for $Q > 0$, finite-time blow-up must occur. For the Fisher–Stefan model (12)–(15) with $\lambda > 0$, we use our observations from Subsection 3.3 to conjecture that finite-time blow-up occurs for $Q > Q_{\text{crit}}$, where $Q_{\text{crit}} < 0$ depends on λ, with $Q_{\text{crit}} \to 0$ as $\lambda \to 0^-$.

For example, the solution in Figure 6C computed for $M(0) = 1$ and $\kappa = -1$ has $Q = 0$. Since $\lambda > 0$ here, our conjecture here is that blow-up will occur if $Q > Q_{\text{crit}}$ where $Q_{\text{crit}} < 0$, including the value $Q = 0$. Therefore, this numerical solution is an example of this type of behavior.

We have already discussed finite-time blow-up in Subsection 2.3. It is worth revisiting the near-blow-up behavior in some detail. For the Stefan problem (12)–(15) with $\lambda = 0$, it is known that

$$\tilde{s}(\tilde{t}) - \tilde{s}_c \sim 2(\tilde{t}_c - \tilde{t})^{1/2} \ln^{1/2}(-\ln(\tilde{t}_c - \tilde{t})) \quad \text{as} \quad \tilde{t} \to \tilde{t}_c^-, \tag{21}$$

which is very close to a $1/2$ power-law dependence but moderated by a very weak logarithm.[55] This complicated scaling can be derived using formal asymptotics via a Biaocchi transform.[56] While this machinery is not appropriate for (12)–(15) with $\lambda > 0$, it is reasonable to postulate that (21) holds for $\lambda > 0$ as well as $\lambda = 0$, since $\partial^2\tilde{u}/\partial\tilde{x}^2 \gg \tilde{u}(1 - \tilde{u})$ in the neighborhood of $\tilde{x} = \tilde{s}(\tilde{t})$ close to the blow-up time.

To support our conjecture that (21) is appropriate for (12)–(15) with $\lambda > 0$, a brief summary of the formal analysis without the Baiocchi transform is as follows. Clearly, $\tilde{u}^2 \ll \tilde{u}$ in the neighborhood of $\tilde{x} = \tilde{s}(\tilde{t})$, thus the important near blow-up behavior is driven by the solution to

$$\frac{\partial\tilde{u}}{\partial\tilde{t}} = \frac{\partial^2\tilde{u}}{\partial\tilde{x}^2} + \lambda\tilde{u}, \quad \tilde{s}(\tilde{t}) - \tilde{x} \ll 1. \tag{22}$$

It is natural to remove linear source term $\lambda\tilde{u}$ in (22) by defining a new independent variable

$$\tilde{v}(\tilde{x},\tilde{t}) = \mathrm{e}^{\lambda(\tilde{t}_\mathrm{c}-\tilde{t})}\,\tilde{u}, \tag{23}$$

so that $\tilde{v}$ satisfies the heat equation subject to

$$\tilde{v} = 0, \quad \frac{d\tilde{s}}{d\tilde{t}} = -\kappa\,\mathrm{e}^{-\lambda(\tilde{t}_\mathrm{c}-\tilde{t})}\frac{\partial\tilde{v}}{\partial\tilde{x}} \quad \text{on} \quad \tilde{x} = \tilde{s}(\tilde{t}). \tag{24}$$

In this way, we can see the close connection between our moving problem with the Fisher–KPP equation and the Stefan problem for the heat equation (see Subsection 3.2).

Indeed, for λ sufficiently small, we follow the ideas by King and Evans [56] for the Stefan problem although, as mentioned, we will not use the Baiocchi transform. First, we look for a solution of the form

$$\tilde{v} \sim \frac{1}{(\tilde{t}_\mathrm{c}-\tilde{t})^a} f(\xi,\tau) \quad \text{as} \quad \tilde{t} \to \tilde{t}_\mathrm{c}^-, \tag{25}$$

where the similarity variables are

$$\xi = \frac{\tilde{x}-\tilde{s}_\mathrm{c}}{(\tilde{t}_\mathrm{c}-\tilde{t})^b}, \quad \tau = -\ln(\tilde{t}_\mathrm{c}-\tilde{t}). \tag{26}$$

Immediately, satisfying the heat equation for $\tilde{v}$ means that $b = 1/2$. The choice $a = 0$ allows a match in the boundary conditions (14). The result is that

$$\tilde{v} \sim f(\xi,\tau) \quad \text{as} \quad \tau \to \infty, \tag{27}$$

where

$$\xi = \frac{\tilde{x}-\tilde{s}_\mathrm{c}}{(\tilde{t}_\mathrm{c}-\tilde{t})^{1/2}}, \quad \tau = -\ln(\tilde{t}_\mathrm{c}-\tilde{t}), \quad \sigma(\tau) = \frac{\tilde{s}(\tilde{t})-\tilde{s}_\mathrm{c}}{(\tilde{t}_\mathrm{c}-\tilde{t})^{1/2}}, \tag{28}$$

and f satisfies

$$\frac{\partial f}{\partial\tau} = \frac{\partial^2 f}{\partial\xi^2} - \frac{1}{2}\xi\frac{\partial f}{\partial\xi}, \quad \xi < \sigma(\tau), \tag{29}$$

$$f = 0, \quad \dot{\sigma} - \frac{1}{2}\sigma = -\kappa\,\mathrm{e}^{-\lambda\exp(-\tau)} f_\xi \quad \text{on} \quad \xi = \sigma(\tau), \tag{30}$$

where the dot means a derivative with respect to τ. The use of self-similar variables ξ and τ in (27)–(28) (instead of just ξ) is discussed at length in Ref. 60, for example.

Before continuing, it is worth explaining that a key reason the analysis for this problem is much more complicated than a traditional similarity solution is that the straightforward ansatz $\tilde{v} \sim f(\xi)$ as $\tau \to \infty$ does not work, as it leads to $f'' - \xi f'/2 = 0$, whose solutions blow up exponentially fast as $\xi \to -\infty$. The culprit is the sign of $\tilde{t}$ in $(\tilde{t}_\mathrm{c}-\tilde{t})^{1/2}$, which leads to an unwanted negative sign when taking the derivative with respect to time. Furthermore, for such a straightforward similarity solution, the moving boundary would be characterized by $\sigma =$ constant, giving $\tilde{s}-\tilde{s}_\mathrm{c} \sim$

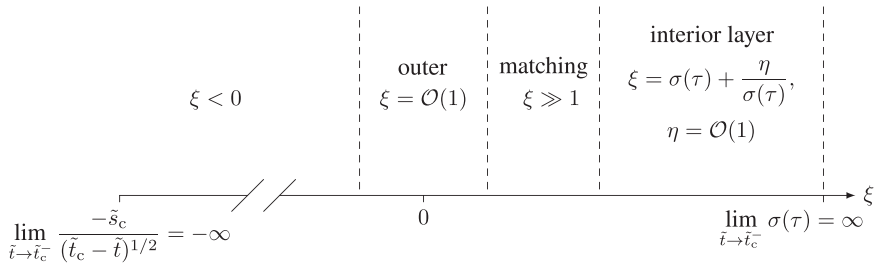

FIGURE 7 A schematic of the structure of the near-blow-up analysis in terms of the variables $\xi = (\tilde{x} - \tilde{s}_c)/(\tilde{t}_c - \tilde{t})^{1/2}$ and $\tau = -\ln(\tilde{t}_c - \tilde{t})$. The diminishingly small region $\tilde{s}_c < \tilde{x} < \tilde{s}(\tilde{t})$ is stretched out to $0 < \xi < \sigma(\tau)$, where $\sigma \to \infty$ as $\tilde{t} \to \tilde{t}_c^-$ ($\tau \to \infty$)

constant $(\tilde{t}_c - \tilde{t})^{1/2}$; however, as stated above in (21), it turns out that $\sigma \to \infty$ (very slowly) in the limit, leading to a complicated spatial structure for ξ in the limit $\tau \to \infty$, as we now summarize. A schematic to help with this description is provided in Figure 7.

Following the key ideas in Ref. 56, for $\xi = \mathcal{O}(1)$ we write

$$f \sim C + A(\tau) + \dot{A}(\tau)\Phi_0(\xi) + \ddot{A}(\tau)\Phi_1(\xi) \quad \text{as} \quad \tau \to \infty, \tag{31}$$

where C is a constant and $A(\tau)$ is an unknown function with the property $|\ddot{A}| \ll |\dot{A}| \ll |A| \ll 1$ as $\tau \to \infty$. By substituting (31) into (29), to leading order we find

$$\Phi_0'' - \frac{1}{2}\xi\Phi_0' = 1. \tag{32}$$

Excluding exponential growth as $\xi \to -\infty$, we find $\Phi_0' = \sqrt{\pi}e^{\xi^2/4}(1 + \text{erf}(\xi/2))$, with the asymptotic behavior $\Phi_0' \sim -2/\xi$ as $\xi \to -\infty$ and $\Phi_0' \sim 2\sqrt{\pi}e^{\xi^2/4} - 2/\xi + 4/\xi^3$ as $\xi \to \infty$. Therefore we have, as a matching condition,

$$\Phi_0 \sim \frac{4\sqrt{\pi}}{\xi} e^{\xi^2/4} \quad \text{as} \quad \xi \to \infty. \tag{33}$$

The solution for Φ_1 is not required in what follows. Note that expansions such as (31), together with an ansatz such as (27)–(28), are used in studies of singularities in other Stefan problems, for example for inward solidification.[61–63]

Near the moving boundary $\xi = \sigma(\tau)$ there is an interior layer with

$$\xi = \sigma + \frac{\eta}{\sigma}, \tag{34}$$

where $\eta = \mathcal{O}(1)$. In this boundary layer, let $f = \Psi(\eta, \tau)$, so that (29) becomes

$$\frac{1}{\sigma^2}\frac{\partial\Psi}{\partial\tau} + \left(-\sigma + \frac{\eta}{\sigma}\right)\frac{\dot{\sigma}}{\sigma^2}\frac{\partial\Psi}{\partial\eta} = \frac{\partial^2\Psi}{\partial\eta^2} - \frac{1}{2}\left(1 + \frac{\eta}{\sigma^2}\right)\frac{\partial\Psi}{\partial\eta}, \quad \eta < 0, \tag{35}$$

which is dominated by the right-hand side in the limit $\tau \to \infty$. We write

$$f \sim \Psi_0(\eta) + \frac{1}{\sigma^2}\Psi_1(\eta) \quad \text{as} \quad \tau \to \infty, \tag{36}$$

so that, after substituting into (35), we find

$$\Psi_0'' - \frac{1}{2}\Psi_0' = 0, \quad \Psi_1'' - \frac{1}{2}\Psi_1' = \frac{1}{2}\eta\Psi_0'. \tag{37}$$

After satisfying the first condition in (30), we find $\Psi_0 = \text{constant}(1 - \mathrm{e}^{\eta/2})$. To determine the constant, we assume that

$$\lambda \exp(-\tau) \ll 1, \quad \text{or} \quad \tilde{t}_c - \tilde{t} \ll \lambda^{-1}, \tag{38}$$

so that the second condition in (30) gives $-1/2 = -\kappa\Psi_0'(0)$, which means

$$\Psi_0 = -\frac{1}{\kappa}(1 - \mathrm{e}^{\eta/2}). \tag{39}$$

The solution for Ψ_1 subject to $\Psi_1 = 0$ and $\Psi_1' = 0$ at $\eta = 0$ (from the first and second conditions in (30), respectively) is

$$\Psi_1 = -\frac{2}{\kappa} + \frac{\eta^2 - 4\eta + 8}{4\kappa}\,\mathrm{e}^{\eta/2}. \tag{40}$$

Matching between the interior layer (36), (39)–(40) and the region for $\xi = \mathcal{O}(1)$, (31), in the limit $\eta \to -\infty$, gives

$$C = -\frac{1}{\kappa}, \quad A \sim -\frac{2}{\kappa\sigma^2}, \tag{41}$$

while matching between the exponential terms in (33) and (39) gives

$$\frac{4\sqrt{\pi}}{\sigma}\,\mathrm{e}^{\sigma^2/4}\dot{A} \sim \frac{1}{\kappa}. \tag{42}$$

Together, these results give

$$\frac{16\sqrt{\pi}}{\kappa\sigma^4}\,\mathrm{e}^{\sigma^2/4}\dot{\sigma} \sim \frac{1}{\kappa}, \quad \text{or} \quad \frac{32\sqrt{\pi}}{\sigma^5}\,\mathrm{e}^{\sigma^2/4} \sim \tau, \quad \text{as} \quad \tau \to \infty. \tag{43}$$

Finally, we find that, to leading order,

$$A \sim -\frac{1}{2\kappa \ln \tau}, \quad \sigma \sim 2\ln^{1/2}\tau, \quad \text{as} \quad \tau \to \infty. \tag{44}$$

The latter implies that $\tilde{s}(\tilde{t}) - \tilde{s}_c \sim 2(\tilde{t}_c - \tilde{t})^{1/2}\ln^{1/2}\tau$, which is (21).

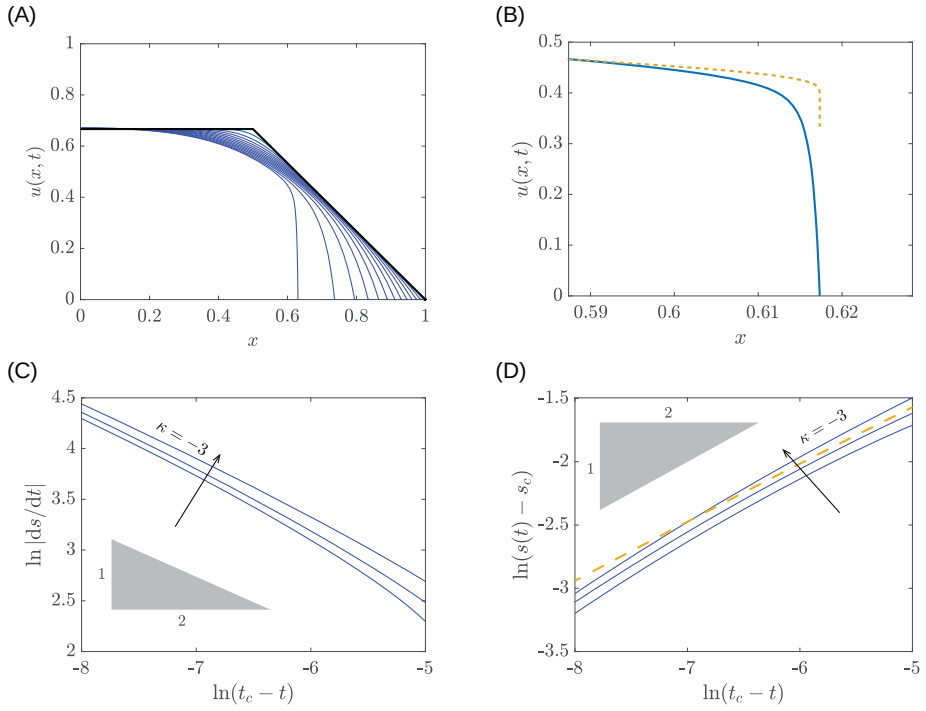

FIGURE 8 (A) Time-dependent solutions of (12)–(15) (in blue) for $\kappa = -3$, $\lambda = 1$ and the ramp style initial condition with $M(0) = 0.5$ (in black). The solutions are drawn at time intervals of 2×10^{-3}. (B) Solution at $\tilde{t}_c \approx 0.024$ (in blue) is compared to (45) (orange dashed) where $\tilde{s}_c = 0.614$. Log–log plots for (C) $d\tilde{s}/d\tilde{t}$ versus $\tilde{t}_c - \tilde{t}$ and (D) $\tilde{s}(\tilde{t}) - \tilde{s}_c$ versus $\tilde{t}_c - \tilde{t}$, drawn for $\kappa = -5, -4, -3$. Arrows indicate increasing values of κ. Also included is a line segment with slope $-1/2$ in (C) and $1/2$ in (D). The near blow-up result (21) is shown in (D) as an orange dashed curve

In the original variables, the blow-up profile has the limiting behavior

$$\tilde{u}(\tilde{x}, \tilde{t}_c) \sim -\frac{1}{\kappa}\left(1 + \frac{1}{2\ln\left(-\ln(\tilde{s}_c - \tilde{x})\right)}\right) \quad \text{as} \quad \tilde{x} \to \tilde{s}_c^-. \tag{45}$$

This is the same limiting profile as for the Stefan problem described in Subsection 3.2. As mentioned above, the key reason that (21) and (45) are unchanged for $\lambda = \mathcal{O}(1)$ when compared to $\lambda = 0$ is that the reaction terms $\lambda\tilde{u}(1 - \tilde{u})$ do not contribute to leading-order behavior near the moving boundary $\tilde{x} = \tilde{s}(\tilde{t})$.

Limits such as (21) and (45) are incredibly difficult to test numerically, as are all blow-up scenarios where the speed of the moving boundary becomes unbounded in a finite time. In this case, it is the double logarithm that grows so slowly that its effect kicks in on time and length scales that are pushing the limits of the numerical scheme. In Figure 8, we show simulations of (12)–(15) for $\lambda = 1$ and values of κ that lead to blow-up. In Figure 8A, solutions are shown for various times for $\tilde{t} > 0$ (in blue), including the initial condition (in black), which is a ramp style function. In Figure 8B, part of a solution profile is drawn close to the estimated blow-up time, again as a solid blue curve, together with (45), which is a thick orange dashed curve. Given the challenges involved in making this comparison, the agreement is quite good.

In terms of the time-dependence of solutions shown in Figure 8A–B, we have included log–log plots of both $d\tilde{s}/d\tilde{t}$ and $\tilde{s}(\tilde{t}) - \tilde{s}_c$ versus $\tilde{t}_c - \tilde{t}$ in Figure 8C,D, respectively, computed for three different values of κ. Included in these images are line segments with slopes $-1/2$ and $1/2$, to indicate the dominant part of the power-law dependence in (21), together with (21) itself. Of course, it is difficult to capture this behavior on very small timescales, especially given the logarithm of the logarithm in (21), which only begins to grow significantly for extremely small values of $\tilde{t}_c - \tilde{t}$. With this in mind, the agreement is acceptable.

4 | DISCUSSION

In this paper, we have studied a Stefan-type moving boundary problem where the usual heat equation is replaced by the Fisher–KPP equation. We refer to this system as the Fisher–Stefan model. From a biological perspective, modifying the Fisher–KPP equation to include a moving boundary has a number of advantages, for example, it allows for solutions with compact support which are more realistic than those that decay exponentially in the far field. This particular advantage is also shared with models that use nonlinear degenerate diffusion for cell motility,[64] for example, resulting in the Porous–Fisher equation,[65–68] without needing to discard linear diffusion. Various other moving boundary problems that are adapted from the Fisher–KPP model have been studied in recent times.[69–72]

The Fisher–Stefan model (1)–(4) involves a new parameter κ, which is a measure of leakage at the moving boundary. This extra parameter allows for a range of qualitative behaviors that are not available for the usual Fisher–KPP model. In particular, for $\kappa > 0$, the moving boundary invades an empty space and, depending on the initial conditions, the solution may evolve to traveling wave or go to extinction. Du and Lin[16] refer to this situation as the spreading-vanishing dichotomy. Aspects of these phenomena have been studied rigorously and numerically by Du and coworkers,[16,28–31,50] us,[27,46–49] and others.

Our study in this paper is for $\kappa < 0$, for which the moving boundary retreats from the empty space (see also Refs. 27, 48). By neglecting the effect of imposing a boundary condition at the left-hand boundary (Section 2), we have used numerical simulation to demonstrate how solutions for $-1 < \kappa < 0$ evolve to retreating traveling waves while those for $\kappa < -1$ blow up in finite time; for the borderline case $\kappa = -1$, it appears that solutions blow up in infinite time. By including the effects of a no-flux condition at the left boundary (Section 3), we eliminate the possibility of traveling wave solutions. Instead, the solution may also exhibit finite-time blow-up for κ less than some critical value, but this critical value depends on the initial condition and the proliferation rate λ. Furthermore, the other option apart from blow-up is extinction, which occurs when the initial population size (or "mass") is sufficiently small. There is a direct analogy here with the problem of melting a superheated solid,[12,52–58] which we describe in some detail.

The finite-time blow-up we report on here involves the speed of the moving boundary and the slope of the solution at the moving boundary both becoming infinite at some time $t_c < \infty$. The population density itself remains bounded in the interval $0 \leq u \leq 1$. One of the reasons why this study is interesting is that blow-up in reaction diffusion equations is more commonly accompanied by the population itself increasing with outbound, for example, where the reaction term is of the form u^p where $p > 1$.[73,74] Blow-up with a bounded dependent variable, as we observe here with a model based on a second-order parabolic partial differential equation, is more likely to be observed in first-order wave equations where shocks are well-known to form.[75]

We have presented a summary of the blow-up asymptotics for the rescaled problem (12)–(15) in Subsection 3.4. After ignoring the nonlinear term $-\tilde{u}^2$, the details follow that for the superheated Stefan problem with $\lambda = 0$ closely,[55,56] although we have presented the analysis without resorting to the Baiocchi transform. A key observation is that the time-dependence (21) relies on (38), which means that if $\lambda = \mathcal{O}(1)$, then (21) provides a good leading-order estimate. However, if $\lambda \gg 1$, then (21) holds for such an incredibly small time interval before blow-up that it is too difficult to test numerically. This is an important observation because, due to (16), our numerical simulations in Figures 1, 3–4 are for $\lambda = 10^6$, which is very large.

In terms of further work, it would be interesting to revisit our numerical results in a rigorous setting. For example, by posing (1)–(4) on $-\infty < x \leq s(t)$, a proof of global existence for $-1 \leq \kappa < 0$ and local existence for $\kappa < -1$ as worth exploring, as is a rigorous exploration of the near blow-up conjecture (21). Furthermore, a proof of our conjecture that the borderline case $\kappa = -1$ corresponds to infinite-time blow-up (on the semi-infinite domain) would be welcome. In terms of extinction, the rough estimate (20) could be refined using careful bounds on the solution with $\lambda > 0$.

Another issue worth further formal investigation is stability. In the Stefan problem (12)–(15) with $\lambda = 0$, when $\kappa > 0$ (normal melting/freezing) the solutions are stable to perturbations in the transverse direction (in the y-direction, say), while for $\kappa < 0$ (melting a superheated solid or freezing a supercooled liquid) the solutions are highly unstable, even with a surface-tension-type regularization.[76] It would be interesting from a mathematical perspective to extend known stability results to the Fisher–Stefan model with a moving boundary. Numerical simulations and linear stability analysis would provide insight whether the front is unstable and which modes grow the fastest, for example. Such an approach would require an analogous restoring force such as surface tension, as included in other moving boundary problems in mathematical biology.[14]

ACKNOWLEDGMENTS

This work is supported by the Australian Research Council (DP200100177). SWM is grateful to John King and Julian Back for discussions on Stefan problems. The authors thank the anonymous referees for their constructive feedback.

REFERENCES

1. Brosa PF, Please CP, Van G. Extended Stefan problem for the solidification of binary alloys in a sphere. *Eur J Appl Math*. 2021;32(2):242-279.
2. Hill JM. *One-Dimensional Stefan Problems: An Introduction*. Longman Scientific & Technical; 1987.
3. McCue SW, Wu B, Hill JM. Classical two–phase Stefan problem for spheres. *Proc R Soc A*. 2008;464:2055-2076.
4. Crank J. *Free and Moving Boundary Problems*. Oxford University Press; 1987.
5. Mitchell SL, O'Brien SBG. Asymptotic and numerical solutions of a free boundary problem for the sorption of a finite amount of solvent into a glassy polymer. *SIAM J Appl Math*. 2014;74:697-723.
6. McCue SW, Hsieh M, Moroney TJ, Nelson MI. Asymptotic and numerical results for a model of solvent-dependent drug diffusion through polymeric spheres. *SIAM J Appl Math*. 2011;71:2287-2311.
7. McGuinness MJ, Please CP, Fowkes N, McGowan P, Ryder L, Forte D. Modelling the wetting and cooking of a single cereal grain. *IMA J Math Appl Bus Ind*. 2000;11:49-70.
8. Gibou F, Fedkiw R, Caflisch R, Osher S. A level set approach for the numerical simulation of dendritic growth. *J Sci Comput*. 2003;19:183-199.
9. Juric D, Tryggvason G. A front-tracking method for dendritic solidification. *J Comput Phys*. 1996;123:127-148.
10. Howison SD. Fingering in Hele-Shaw cells. *J. Fluid Mech*. 1986;167:439-453.
11. Langer JS. Dendrites, viscous fingers, and the theory of pattern formation. *Science*. 1989;243:1150-1156.

12. Howison SD, Ockendon JR, Lacey AA. Singularity development in moving-boundary problems. *Q J Mech Appl Math*. 1985;38:343-360.
13. Franks SJ, King JR. Interactions between a uniformly proliferating tumour and its surroundings: uniform material properties. *Math Med Biol*. 2003;20:47-89.
14. Giverso C, Verani M, Ciarletta P. Branching instability in expanding bacterial colonies. *J R Soc Interface*. 2015;12:20141290.
15. Ward JP, King JR, Koerber AJ, Croft JM, Sockett RE, Williams P. Early development and quorum sensing in bacterial biofilms. *J Math Biol*. 2003;47:23-55.
16. Du Y, Lin Z. Spreading–vanishing dichotomy in the diffusive logistic model with a free boundary. *SIAM J Math Anal*. 2010;42:377-405.
17. Fisher RA. The wave of advance of advantageous genes. *Ann Eugen*. 1937;7:355-369.
18. Kolmogorov AN, Petrovskii PG, Piskunov NS. A study of the diffusion equation with increase in the amount of substance, and its application to a biological problem. *Moscow Univ Math Bull*. 1937;1:1-26.
19. Edelstein-Keshet L. *Mathematical Models in Biology*. SIAM; 2005.
20. Murray JD. *Mathematical Biology I: An Introduction*. 3rd ed. Springer; 2002.
21. Jin W, Shah ET, Penington CJ, McCue SW, Chopin LK, Simpson MJ. Reproducibility of scratch assays is affected by the initial degree of confluence: experiments, modelling and model selection. *J Theor Biol*. 2016;390:136-145.
22. Jin W, Shah ET, Penington CJ, McCue SW, Maini PK, Simpson MJ. Logistic proliferation of cells in scratch assays is delayed. *Bull Math Biol*. 2017;79:1028-1050.
23. Jin W, Lo K-Y, Chou S-E, McCue SW, Simpson MJ. The role of initial geometry in experimental models of wound closing. *Chem Eng Sci*. 2018;179:221-226.
24. Johnston ST, Shah ET, Chopin LK, McElwain DLS, Simpson MJ. Estimating cell diffusivity and cell proliferation rate by interpreting IncuCyte ZOOM^{TM} assay data using the Fisher–Kolmogorov model. *BMC Syst Biol*. 2015;9:38:1-38:12.
25. Maini PK, McElwain DLS, Leavesley D. Traveling waves in a wound healing assay. *Appl Math Lett*. 2004;17:575-580.
26. Warne DJ, Baker RE, Simpson MJ. Using experimental data and information criteria to guide model selection for reaction–diffusion problems in mathematical biology. *Bull Math Biol*. 2019;81:1760-1804.
27. El-Hachem M, McCue SW, Simpson MJ. Invading and receding sharp-fronted travelling waves. *Bull Math Biol*. 2021;83:35.
28. Du Y, Matano H, Wang K. Regularity and asymptotic behavior of nonlinear Stefan problems. *Arch Ration Mech Anal*. 2014;212:957-1010.
29. Du Y, Matsuzawa H, Zhou M. Sharp estimate of the spreading speed determined by nonlinear free boundary problems. *SIAM J Math Anal*. 2014;46:375-396.
30. Du Y, Lou B. Spreading and vanishing in nonlinear diffusion problems with free boundaries. *J Eur Math Soc*. 2015;17:2673-2724.
31. Du Y. Propagation, diffusion and free boundaries. *SN Partial Differ Equ Appl*. 2020;1:35.
32. Bao W, Du Y, Lin Z, Zhu H. Free boundary models for mosquito range movement driven by climate warming. *J Math Biol*. 2018;76:841-875.
33. Cai J, Gu H. Asymptotic behavior of solutions of free boundary problems for Fisher–KPP equation. *Eur J Appl Math*. 2017;28:435-469.
34. Cai J, Xu L. Asymptotic behaviour of solutions of Fisher–KPP equation with free boundaries in time-periodic environment. *Eur J Appl Math*. 2020;31:423-449.
35. Cao JF, Du Y, Li F, Li WT. The dynamics of a Fisher–KPP nonlocal diffusion model with free boundaries. *J Funct Anal*. 2019;277:2772-2814.
36. Chang C-H, Chen C-C, Huang C-C. Traveling wave solutions of a free boundary problem with latent heat effect. *Discrete Continuous Dyn Syst Ser B*. 2021;26:1797-1809.
37. Ding W, Du Y, Guo Z. The Stefan problem for the Fisher–KPP equation with unbounded initial range. *Calc Var Partial Differ Equ*. 2021;60:69.
38. Du Y, Wu CH. Spreading with two speeds and mass segregation in a diffusive competition system with free boundaries. *Calc Var Partial Differ. Equ*. 2018;57:52.

39. Endo M, Kaneko Y, Yamada Y. Free boundary problem for a reaction–diffusion equation with positive bistable nonlinearity. *Discrete Continuous Dyn Syst Ser A*. 2020;40:3375-3394.
40. Jiang D-H, Wang Z-C. The diffusive logistic equation on periodically evolving domains. *J Math Anal Appl*. 2018;458:93-111.
41. Kaneko Y, Yamada Y. Spreading speed and profiles of solutions to a free boundary problem with Dirichlet boundary conditions. *J Math Anal Appl*. 2018;465:1159-1175.
42. Lutscher F, Fink J, Zhu Y. Pushing the boundaries: models for the spatial spread of ecosystem engineers. *Bull Math Biol*. 2020;82:138.
43. Wang RH, Wang L, Wang ZC. Free boundary problem of a reaction-diffusion equation with nonlinear convection term. *J Math Anal Appl*. 2018;467:1233-1257.
44. Wang M. Existence and uniqueness of solutions of free boundary problems in heterogeneous environments. *Discrete Continuous Dyn Syst Ser B*. 2019;24:415-421.
45. Yuan J, Huang J. Blowup and vanishing of a free boundary problem with a nonlocal reaction term. *Appl Anal*. 2021. https://doi.org/10.1080/00036811.2020.1869940
46. El-Hachem M, McCue SW, Jin W, Du Y, Simpson MJ. Revisiting the Fisher–Kolmogorov–Petrovsky–Piskunov equation to interpret the spreading–extinction dichotomy. *Proc R Soc A*. 2019;475:20190378.
47. El-Hachem M, McCue SW, Simpson MJ. A sharp-front moving boundary model for malignant invasion. *Physica D*. 2020;412:132639.
48. McCue SW, El-Hachem M, Simpson MJ. Exact sharp-fronted travelling wave solutions of the Fisher–KPP equation. *Appl Math Lett*. 2021;114:106918.
49. Simpson MJ. Critical length for the spreading-vanishing dichotomy in higher dimensions. *ANZIAM J*. 2020;62:3-17.
50. Liu S, Du Y, Liu X. Numerical studies of a class of reaction-diffusion equations with Stefan conditions. *Int J Comput Math*. 2020;97:959-979.
51. Ablowitz M, Zeppetella A. Explicit solutions of Fisher's equation for a special wave speed. *Bull Math Biol*. 1979;41:835-840.
52. Back JM, McCue SW, Moroney TJ. Numerical study of two ill-posed one phase Stefan problems. *ANZIAM J*. 2010;52:430-446.
53. Fasano A, Primicerio M. General free-boundary problems for the heat equation I. *J Math Anal Appl*. 1977;57:694-723.
54. Fasano A, Primicerio M, Lacey AA. New results on some classical parabolic free-boundary problems. *Q Appl Math*. 1981;38:439-460.
55. Herrero MA, Velázquez JJL. Singularity formation in the one-dimensional supercooled Stefan problem. *Eur J Appl Math*. 1996;7:119-150.
56. King JR, Evans JD. Regularization by kinetic undercooling of blow-up in the ill-posed Stefan problem. *SIAM J Appl Math*. 2005;65:1677-1707.
57. Lacey AA, Ockenson JR. Ill-posed free boundary problems. *Control Cybern*. 1985;296:C432-C433.
58. Sherman B. A general one-phase Stefan problem. *Q Appl Math*. 1970;28:377-382.
59. Skellam JG. Random dispersal in theoretical populations. *Biometrika*. 1951;38:196-218.
60. Eggers J, Fontelos MA. The role of self-similarity in singularities of partial differential equations. *Nonlinearity*. 2009;22:R1-R44.
61. Herrero MA, Velázquez JJL. On the melting of ice ball. *SIAM J Math Anal*. 1997;28:1-32.
62. McCue SW, King JR, Riley DS. The extinction problem for three-dimensional inward solidification. *J Eng Math*. 2005;52:389-409.
63. Soward AM. A unified approach to Stefan's problem for spheres. *Proc R Soc A*. 1980;373:131-147.
64. Simpson MJ, Baker RE, McCue SW. Models of collective cell spreading with variable cell aspect ratio: a motivation for degenerate diffusion models. *Phys Rev E*. 2011;83:021901.
65. Fadai, NT, Simpson MJ. New travelling wave solutions of the Porous–Fisher model with a moving boundary. *J Phys A Math Theor*. 2020;53:095601.
66. McCue SW, Jin W, Moroney TJ, Lo K-Y, Chou SE, Simpson MJ. Hole-closing model reveals exponents for nonlinear degenerate diffusivity functions in cell biology. *Physica D*. 2019;398:130-140.
67. Sánchez Garduno F, Maini PK. Traveling wave phenomena in some degenerate reaction-diffusion equations. *J Differ Equ*. 1994;117:281-319.

68. Witelski TP. Merging traveling waves for the porous-Fisher's equation. *Appl Math Lett*. 1995;8:57-62.
69. Berestycki J, Brunet É, Derrida B. Exact solution and precise asymptotics of a Fisher–KPP type front. *J Phys A Math Theor*. 2018;51:035204.
70. Berestycki J, Brunet É, Penington S. Global existence for a free boundary problem of Fisher–KPP type. *Nonlinearity*. 2019;32:3912-3939.
71. Berestycki J, Brunet É, Penington S. A free boundary problem arising from branching Brownian motion with selection. *Trans Am Math Soc*. 2021;374:6269-6329.
72. Tisbury ADO, Needham DJ, Tzella A. The evolution of traveling waves in a KPP reaction-diffusion model with cut-off reaction rate. I. Permanent form traveling waves. *Stud Appl Math*. 2021;146:301-329.
73. Deng K, Levine HA. The role of critical exponents in blow-up theorems: the sequel. *J Math Anal Appl*. 2000;243:85-126.
74. Levine HA. The role of critical exponents in blowup theorems. *SIAM Rev*. 1990;32:262-288.
75. Whitham GB. *Linear and Nonlinear Waves*. Wiley; 2011.
76. Mullins WW, Sekerka RF. Morphological stability of a particle growing by diffusion or heat flow. *J Appl Phys*. 1963;34:323-329.

How to cite this article: McCue SW, El-Hachem M, Simpson MJ. Traveling waves, blow-up, and extinction in the Fisher–Stefan model. *Stud Appl Math*. 2022;148:964–986. https://doi.org/10.1111/sapm.12465

APPENDIX A: NUMERICAL METHODS

To obtain numerical solutions of the Fisher–Stefan equation

$$\frac{\partial u}{\partial t} = \frac{\partial^2 u}{\partial x^2} + \lambda u(1-u), \tag{A1}$$

for $0 < x < s(t)$ and $t > 0$, we use a boundary fixing transformation $y = x/s(t)$ so that we have

$$\frac{\partial u}{\partial t} = \frac{1}{s^2(t)}\frac{\partial^2 u}{\partial y^2} + \frac{y}{s(t)}\frac{ds(t)}{dt}\frac{\partial u}{\partial y} + \lambda u(1-u), \tag{A2}$$

on the fixed domain, $0 < y < 1$. Here, $s(t)$ is the time-dependent length of the domain, and we will explain how we solve for this quantity later. To close the problem, we also transform the boundary conditions giving

$$\frac{\partial u}{\partial y} = 0 \quad \text{at} \quad y = 0, \tag{A3}$$

$$u = 0 \quad \text{at} \quad y = 1. \tag{A4}$$

The key to obtaining accurate numerical solutions of Equation (A1) is to take advantage of the fact that for many problems we consider $u(x,t)$ varies rapidly near $x = s(t)$, whereas $u(x,t)$ is approximately constant near $x = 0$. Motivated by this spatial structure, we discretize Equation (A2) using a variable mesh where the mesh spacing varies geometrically from $\delta y_{\min} = y_N - y_{N-1} = 1 - y_{N-1}$ at $y = 1$, to $\delta y_{\max} = y_2 - y_1 = y_2 - 0$ at $y = 0$. Results in this work are computed with $N = 1001$ mesh points with $\delta y_{\min} = 1 \times 10^{-6}$. With these constraints we solve for the

geometric expansion factor using MATLABs *fsolve* function which gives $\delta y_{\max} = 9.083 \times 10^{-2}$ and the geometric expansion factor is 1.009165 to six decimal places.

We spatially discretize equation (A2) on the nonuniform mesh. At the ith internal mesh point, we define $h_i^+ = y_{i+1} - y_i$ and $h_i^- = y_i - y_{i-1}$. For convenience, we define $\alpha_i = 1/(h^-[h^+ + h^-])$, $\gamma_i = -1/(h^- h^+)$ and $\delta_i = 1/(h^+[h^+ + h^-])$, which gives

$$\begin{aligned}\frac{u_i^{j+1} - u_i^j}{\Delta t} = {} & \frac{2}{(s^j)^2}\left[\alpha_i u_{i-1}^{j+1} + \gamma_i u_i^{j+1} + \delta_i u_{i+1}^{j+1}\right] \\ & + \frac{y_i}{s^j}\left(\frac{s^{j+1} - s^j}{\Delta t}\right)\left[\delta_i h^N u_{i-1}^{j+1} + \gamma_i (h^N - h^+) u_{i-1}^{j+1} - \alpha_i h^+ u_{i+1}^{j+1}\right] \\ & + \lambda u_i^{j+1}\left(1 - u_i^{j+1}\right) \end{aligned} \tag{A5}$$

for $i = 2, \ldots, N-1$, where N is the total number of spatial nodes on the finite difference mesh, and the index j represents the time index so that $u_i^j \approx u(y_i, j\Delta t)$. Finally, discretizing Equations (A3)–(A4) leads to

$$u_2^{j+1} - u_1^{j+1} = 0, \tag{A6}$$

$$u_N^{j+1} = 0. \tag{A7}$$

To advance the discrete system from time t to $t + \Delta t$, we solve the system of nonlinear algebraic equations, Equations (A5)–(A7), using Newton–Raphson iteration. During each iteration of the Newton–Raphson algorithm, we estimate the position of the moving boundary using the discretized Stefan condition. Here, we define $h_N^+ = y_N - y_{N-1}$, $h_N^- = y_{N-1} - y_{N-2}$, $\alpha_N = 1/(h^-[h^+ + h^-])$, and $\gamma_N = -1/(h^- h^+)$, which gives

$$s^{j+1} = s^j - \frac{\Delta t \kappa}{s^j}\left[\alpha_N h^+ u_{N-1}^{j+1} + \gamma_N (h^+ + h^-) u_N^{j+1}\right]. \tag{A8}$$

Within each time step Newton–Raphson iterations continue until the maximum change in the dependent variables is less than the tolerance ϵ. All results in this work are obtained by setting $\epsilon = 1 \times 10^{-10}$, and $\Delta t = 1 \times 10^{-4}$, and we find that these values are sufficient to produce grid-independent results. Software written in MATLAB is available on GitHub for the reader to experiment with different choices of discretization and tolerance values.